JOURNAL OF CATALYSIS 145, 300–311 (1994)

Influence of Precursors Used in Preparation of MgO on Its Surface Properties and Catalytic Activity in Oxidative Coupling of Methane

V. R. Choudhary,[1] V. H. Rane, and R. V. Gadre

Chemical Engineering Division, National Chemical Laboratory, Pune 411 008, India

Received March 25, 1993; revised August 13, 1993

Surface properties (viz., acidity/acid strength distribution, basicity/base strength distribution, surface area, morphology, and surface composition) and catalytic activity/selectivity in the oxidative coupling of methane at different process conditions [reaction temperature, 700–800°C; CH_4/O_2 ratio, 3.0–8.0; and gas hourly space velocity (GHSV), 25,500–102,000 $cm^3 \cdot g^{-1} \cdot h^{-1}$)] of MgO obtained by thermal decomposition of hydrated MgO, magnesium hydroxide, magnesium nitrate, magnesium acetate, and magnesium carbonate have been investigated. The surface and catalytic properties are found to be strongly affected by the precursors used in the preparation of MgO. The catalytic activity and selectivity (for ethane and ethylene) of MgO obtained from magnesium carbonate and magnesium acetate are comparable and are much higher than that observed for MgO obtained from the other precursors.

INTRODUCTION

Most of the catalysts used for the oxidative coupling of methane (OCM) to ethane and ethylene (which is a process of great practical importance in the future) are based on magnesium oxide promoted with alkali metals (1–10), rare earth metals (11–14), lead (15–17), Zn (18), Mn (19), metal chlorides (8, 20, 21), etc. Since MgO is a main component of the promoted MgO catalysts, their catalytic activity/selectivity in the OCM process is expected to be strongly influenced by the properties of MgO in the catalysts.

Active MgO can be prepared by thermal decomposition of magnesium compounds such as Mg hydroxide, Mg carbonate, Mg nitrate, Mg acetate, etc., under controlled conditions. The influence of pretreatment time, temperature, gas environment, and outgassing procedures on sample morphology and surface uniformity of magnesium oxide prepared by dehydration of magnesium hydroxide obtained from different sources has been investigated previously (22). Magnesium oxide prepared under identical conditions from different samples of magnesium hydroxide showed different properties (22, 23). Recently, Choudhary *et al.* have found that the properties (viz., surface area and basicity/base strength distribution) of magnesium oxide obtained from magnesium hydroxide (24) and magnesium carbonate (25) depend strongly upon the magnesium salt and the precipitating agent used for preparing magnesium hydroxide and magnesium carbonate, the precipitation conditions (i.e., concentration of magnesium salt, pH, temperature, and mode of mixing of the salt solution and precipitating agent), the aging period of the precipitated magnesium hydroxide and magnesium carbonate, and on the calcination temperature.

Because of the importance of MgO as a main catalyst constituent in a number of promising catalysts reported for the OCM process, there is great interest in carrying out a detailed investigation on MgO obtained from different precursors (viz., hydrated MgO, magnesium acetate, magnesium hydroxide, magnesium nitrate, and magnesium carbonate) by thermal decomposition. Surface properties (viz., surface area, acidity/acid strength distribution, and basicity/base strength distribution) and catalytic activity/selectivity in the OCM process are of interest. The present investigation was undertaken for this purpose.

EXPERIMENTAL

The MgO (I–VI) catalysts from different precursors, viz., hydrated MgO, magnesium acetate, magnesium nitrate, magnesium hydroxide, and magnesium carbonate (I) and (II), were prepared by thermal decomposition of the catalyst precursors. The catalyst precursors were obtained as follows. The hydrated MgO was prepared by treating powdered MgO (GR, Loba) with deionized water on water bath for 4 h and drying the slurry at 120°C for 12 h. The magnesium acetate (AR, Thomson Backer) and magnesium nitrate (AR, BDH) were ground in deionized water, sufficiently to form a thick paste, and dried at 120°C for 12 h. The magnesium hydroxide, magnesium carbonate (I), and magnesium carbonate (II) were prepared by precipitating them from an aqueous solution

[1] To whom correspondence should be addressed.

0021-9517/94 $5.00

of magnesium nitrate by ammonium hydroxide solution, ammonium carbonate, and sodium carbonate, respectively, at pH 10–11 at 30°C, washing the precipitate with deionized water until free from cations and anions, and then drying at 120°C for 12 h. The dried catalyst precursor mass was decomposed at 600°C for 2 h in static air and then pressed binder-free, crushed to 22–30 mesh size particles, and then calcined at different temperatures (i.e., 600, 750, and 900°C) for 2 h in static air. The temperature was raised at a rate of about 30°C · min^{-1}.

Before measurements were carried out, the catalysts were pretreated *in situ* at their calcination temperature in a flow of moisture-free N_2 (20 cm^3 · min^{-1}) for 1 h.

The surface area of the catalysts was determined by the single-point BET method by measuring the adsorption of N_2 (30 mol%, balance He) at liquid-nitrogen temperature, using a Monosorb Surface Area Analyser (Quantachrome Corp.). The crystal size and morphology of the catalysts were studied by scanning electron microscope (SEM). The surface oxygen, carbon, and magnesium species were studied by X-ray photoelectron spectroscopy (XPS) using a VG-Scientific ESCA-3 MKII electron spectrometer (C (1*s*) with a binding energy of 285 eV was used as an internal standard).

The surface acidity of the MgO samples was determined by temperature-programmed desorption (TPD) of ammonia (chemisorbed at 100°C) from 50 to 900°C in a quartz reactor (packed with 0.5 g catalyst) at a linear heating rate of 20°C · min^{-1} in a flow of moisture-free helium (20 cm^3 · min^{-1}). The ammonia desorbed in the TPD run was detected by a thermal conductivity detector and also measured quantitatively by a chemical analysis (26).

The surface basicity and base strength distribution on the MgO samples were determined by step-wise thermal desorption (STD) of CO_2 (chemisorbed at 50°C) on the catalyst (0.5 g), packed in a quartz reactor, from 50 to 980°C in a number of successive temperature steps (50–250°C, 250–500°C, 500–700°C, and 700°–980°C) and measuring the desorbed CO_2 quantitatively. When the maximum temperature of the respective step was attained it was maintained for a period of 30 min to desorb the CO_2 adsorbed reversibly on the catalyst at that temperature. The detailed procedures for measuring the base strength distribution by the STD of CO_2 and the estimation of CO_2 chemisorption data from the STD data have been described previously (26, 27). The data of STD and chemisorption of CO_2 reported in this paper are presented after subtracting from them the CO_2 content data of the catalyst, which was determined by measuring quantitatively the CO_2 evolved when the catalyst (after its pretreatment at the calcination temperature in the flow of N_2 for 1 h) was heated from room temperature to 1000°C in a flow of pure N_2 for 1 h.

Throughout this paper, the chemisorption is considered as the amount of adsorbate retained by the presaturated catalyst after it was swept with pure He or N_2 for a period of 30 min.

TABLE 1

Properties of MgO Prepared from Different Precursors

Catalyst	Catalyst precursor	Calcination temperature (°C)	Surface area ($m^2 \cdot g^{-1}$)	CO_2 content (mmol · g^{-1})
MgO (I)	Hydrated MgO	600	117.1	0.0
		750	43.6	0.0
		900	14.5	0.0
MgO (II)	Magnesium acetate	600	15.6	1.061
		750	15.0	0.153
		900	11.9	0.055
MgO (III)	Magnesium nitrate	600	8.7	0.0
		750	6.3	0.0
		900	5.1	0.0
MgO (IV)	Magnesium hydroxide	600	68.6	0.0
		750	56.0	0.0
		900	55.6	0.0
MgO (V)	Magnesium carbonate (I)	600	73.1	0.036
		750	60.4	0.018
		900	36.0	0.004
MgO (VI)	Magnesium carbonate (II)	600	76.9	0.050
		750	51.9	0.022
		900	40.7	0.006

The OCM reaction over the MgO catalysts (calcined at 900°C) was carried out in a continuous flow quartz reactor (i.d., 10 mm) provided with a chromel–alumel thermocouple. The catalyst was pretreated *in situ* in a flow of N_2 (30 cm^3 · min^{-1}) at 900°C for 1 h. The feed was a mixture of pure methane and oxygen. The reaction was carried out at the following reaction conditions: amount of catalyst, 0.1 g; gas hourly space velocity (GHSV), 25,500–102,000 cm^3 · g^{-1} · h^{-1}; CH_4/O_2 ratio in feed, 3.0–8.0; and reaction temperature, 700–850°C. The reactor effluent gases, after the removal of water by condensation, were analysed by an on-line gas chromatograph using Porapak-Q and Spherocarb columns.

RESULTS AND DISCUSSION

Catalyst Characterization

The surface area (Table 1) of MgO (I–VI) catalysts decreased with increasing calcination temperature. This is expected due to sintering of MgO at the higher temperatures, causing an increase in the crystal size. The surface area of MgO (I) (calcined at 600°C) is much higher but it decreased sharply with increasing calcination temperature, whereas in the case of MgO (II) the influence of calcination temperature is very small.

The catalysts are arranged in order of their surface area, as follows:

Catalysts calcined at 600°C:

$$\text{MgO(I)} \gg \text{MgO(VI)} > \text{MgO(V)} > \text{MgO(IV)} \gg \text{MgO(II)} > \text{MgO(III)}.$$

Catalysts calcined at 750°C:

$$\text{MgO(V)} > \text{MgO(IV)} > \text{MgO(VI)} > \text{MgO(I)} \gg \text{MgO(II)} > \text{MgO(III)}.$$

Catalysts calcined at 900°C:

$$\text{MgO(IV)} > \text{MgO(VI)} > \text{MgO(V)} \gg \text{MgO(I)} > \text{MgO(II)} > \text{MgO(III)}.$$

The above comparison shows that the order of the catalysts, except MgO (II) and (III), changes with the calcination temperature.

The CO_2 content (i.e., the amount of CO_2 retained after calcination) of MgO (II), (V), and (VI) catalysts (obtained from magnesium acetate and magnesium carbonate by their calcination at 600, 750, and 900°C) is given in Table 1. The CO_2 content of the MgO catalysts (I), (III), and (IV) was found to be negligibly small (<0.001 mmol. g^{-1}). The CO_2 content is higher for the MgO (II) catalyst prepared from magnesium acetate. For catalysts retaining CO_2, the CO_2 content is decreased sharply with increasing the calcination temperature. The high CO_2 content of these catalysts, particularly at lower calcination temperatures, is due to an incomplete decomposition of the catalyst precursor (Mg acetate and Mg carbonate) and/or strong chemisorption of CO_2 (formed in the decomposition of the catalyst precursor) on the basic sites (viz., low coordinated surface O^{2-}) of the catalysts.

The XRD spectra of MgO (II) catalyst, prepared from magnesium acetate by calcination at 600 and 750°C, show a presence of MgO (major) and Mg carbonate (minor or in traces) phases, whereas in MgO (II) calcined at 900°C, only pure MgO phase was observed. The Mg-carbonate phase in the MgO (II) catalyst is found to decrease with increasing calcination temperature. This is consistent with the observed CO_2 content of the catalysts. To the contrary, in the MgO (I), (II), and (V) catalysts calcined at 900°C, the presence of only a magnesium oxide phase was observed. The XRD spectra of the MgO (III), (IV), and (VI) calcined at 900°C, indicated the presence of only the MgO phase. The XRD spectra are given elsewhere (28).

The XPS spectra for C (1*s*) and O (1*s*) of the MgO (I), (II), (IV), and (V) catalysts calcined at 900°C are presented in Fig. 1. The XPS data are given in Table 2. In the C (1*s*) spectra of the catalysts (Fig. 1a), the predominant peak at 285 eV corresponds to residual hydrocarbons, whereas the shoulder peak corresponding to higher electron binding energy for MgO (II) and (V) indicates the presence of carbonate (CO_3^{2-}) species on the catalyst surface. The surface carbonate species are expected to be formed due to chemisorption of CO_2 formed during the decomposition of the catalyst precursors. Figure 1b shows that the O (1*s*) spectra of the MgO (I), (II), (IV), and (V) catalysts are asymmetric and quite broad ($\Delta E_{1/2} \simeq 4.0$ eV), indicating the presence of different surface oxygen species on the catalysts. Earlier ESR studies (29–31) have also indicated the presence of different oxygen species such as O^-, O_2^-, and O^{2-} on MgO.

TABLE 2

XPS Data for MgO Catalysts (Calcined at 900°C)

	C (1*s*)		O (1*s*)		Mg (2*p*)	
Catalyst	E_b (eV)	$E_{1/2}$ (eV)	E_b (eV)	$E_{1/2}$ (eV)	E_b (eV)	$E_{1/2}$ (eV)
MgO (I)	285.0	2.3	530.2	3.6	49.7	2.2
MgO (II)	285.0	2.7	530.1	4.0	50.3	2.4
	289.8	1.6	—	—	—	—
MgO (IV)	285.0	2.5	529.9	3.9	49.3	2.4
MgO (V)	285.0	3.0	530.3	4.3	49.1	2.8
	289.5	2.0	—	—	—	—

Note. E_b = Electron binding energy and $E_{1/2}$ = peak width at half height.

A comparison of the SEM photograph of MgO (I–VI) (calcined at 900°C) is made in Fig. 2. The comparison reveals that the size and morphology of the crystals/particles of MgO produced are very strongly influenced by the catalyst precursor. The catalysts are arranged in the order of their crystal size as follows:

$$\text{MgO(III)} > \text{MgO(II)} > \text{MgO(I)} > \text{MgO(V)} > \text{MgO(VI)} > \text{MgO(IV)}.$$

As expected, this order for the crystal size is exactly the opposite of that for the surface area of the catalysts (calcined at 900°C).

The acid strength distribution on the catalysts (calcined at 900°C) was determined by the TPD of ammonia (chemisorbed at 100°C) from 50–900°C at a linear heating rate of 20°C · min^{-1} using helium as a carrier gas. The TPD curves along with the initial surface coverage (θ_i) by the NH_3 chemisorbed at 100°C on the catalysts are presented in Fig. 3.

The values of the NH_3 chemisorption at 100°C on the catalysts are as follows:

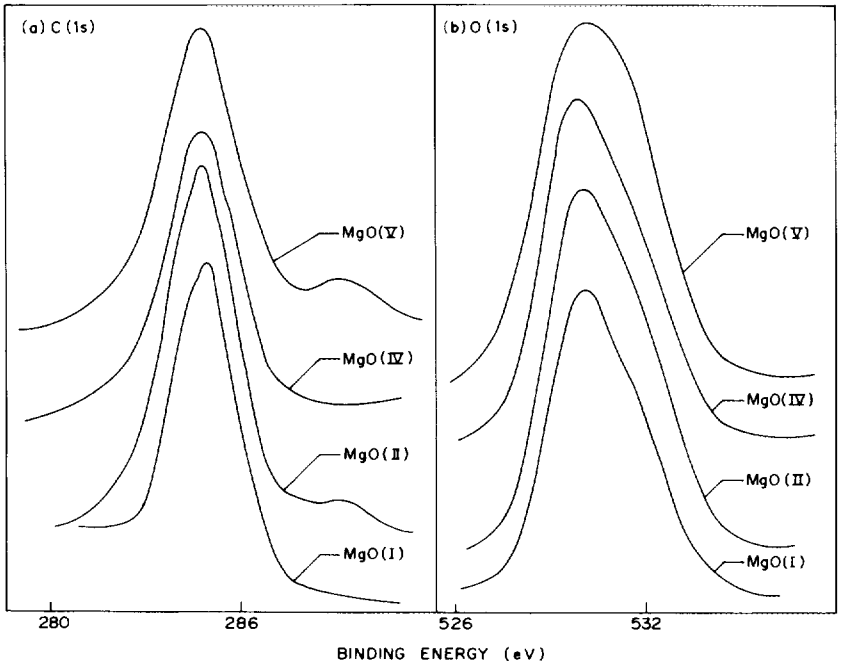

FIG. 1. XPS spectra [C(1*s*) and O(1*s*)] of MgO catalysts (calcined at 900°C).

MgO catalyst (calcined at 900°C):					
I	II	III	IV	V	VI
NH_3 chemisorbed at 100°C (mmol · g^{-1}):					
0.23	0.04	0.11	0.06	0.22	0.11

The results indicate that the total acidity (measured in terms of NH_3 chemisorbed at 100°C) of MgO catalysts is strongly influenced by the precursors used in the catalyst preparation. The total acidity of the MgO catalysts is in the following order:

$$\text{MgO(I)} \simeq \text{MgO(V)} > \text{MgO(III)} \simeq \text{MgO(VI)} > \text{MgO(IV)} \geq \text{MgO(II)}.$$

The TPD curves (Fig. 3) show that the acidity distribution for all the MgO catalysts except for MgO (I) is broad and it is strongly influenced by the precursor used in the catalyst preparation. A comparison of the TPD curves reveals the followings. The main TPD peaks are in three temperature regions: lower temperature (below 250°C), intermediate temperature (300–450°C) and higher temperature (above 500°C), with a peak maximum temperature of about 200, 400, and 650°C, corresponding to α (weak), β (intermediate strength), and γ (strong) acid sites, respectively, on the MgO catalysts. The relative concentrations of the α, β, and γ sites and also their strenghts vary from catalyst to catalyst, depending upon the precursor used in the catalyst preparation. The MgO (I) contains of mainly weak (α) acid sites with a small amount of intermediate strength (β) acid sites, indicated by the major TPD peak at about 200°C with a small hump at about 400°C. The other catalysts contains mainly intermediate strength (β) acid sites with smaller amounts of both the strong (γ) and weak (α) acid sites.

The basicity and base strength distribution on the MgO (I–VI) catalysts calcined at 600, 750, and 900°C have been determined by the STD of CO_2 (chemisorbed at 50°C) from 50–980°C in different temperature steps.

The columns in Fig. 4 show the energy distribution of the sites involved in the chemisorption of CO_2 at the lowest temperature of the STD (i.e., 50°C). Each column represents the number of sites measured in terms of CO_2 desorbed during the corresponding temperature step. The strength of these acid sites is expressed in terms of the desorption temperature of CO_2, T_d, which lies in the range in which the CO_2 chemisorbed at the lowest temperature of the step is desorbed. The sites of strength $T_1 < T_d \leq T_2$ could be obtained from the amount of CO_2 which was initially chemisorbed at T_1 and subsequently desorbed when the temperature was increased from T_1 to T_2.

The chemisorption of CO_2 at a higher temperature points to an involvement of stronger sites. The CO_2 chemisorption vs temperature curves (Fig. 5), therefore, present the type of site energy distribution in which the number of sites are expressed in terms of the amount of CO_2 chemisorbed as a function of chemisorption temperature.

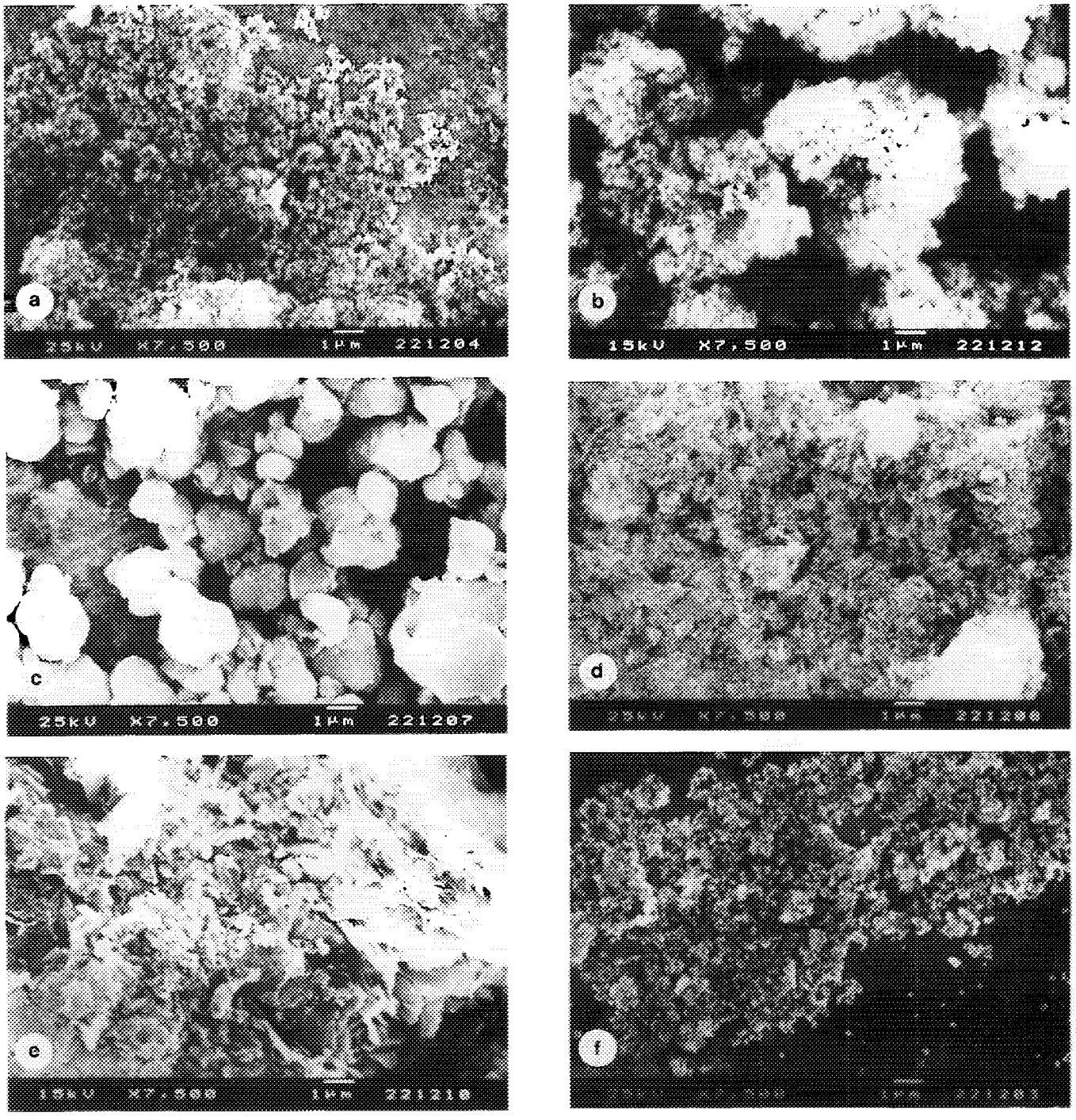

FIG. 2. SEM photographs of MgO (I–VI) catalysts (calcined at 900°C in static air for 2 h): (a) MgO(I), (b) MgO(II), (c) MgO(III), (d) MgO(IV), (e) MgO(V), and (f) MgO(VI).

The basicity distribution and temperature dependence of chemisorption of CO_2 on the catalyst (calcined at 600, 750, and 900°C) are shown in Figs. 4 and 5, respectively.

The results (Figs. 4 and 5) indicate that the base strength distribution on the catalysts is very broad and is strongly influenced by the calcination temperature and precursor used in the preparation of MgO. The catalysts can be arranged for total surface basicity (measured in terms of CO_2 chemisorbed at 50°C) and strong basicity (measured in terms of CO_2 chemisorbed at 500°C), as follows:

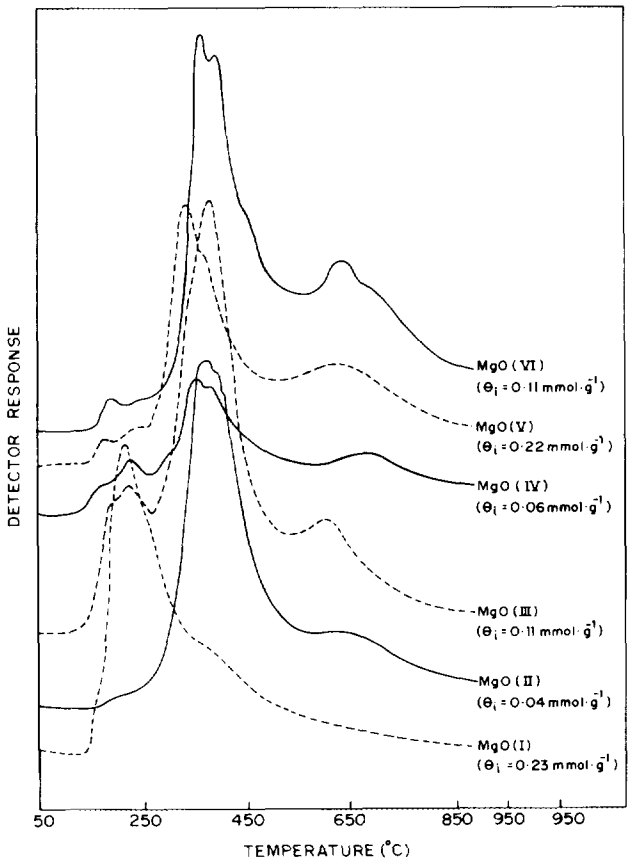

FIG. 3. TPD of ammonia on MgO (I–VI) catalysts calcined at 900°C (θ_i = initial loading of NH_3 on catalyst).

Catalysts calcined at 600°C:

For total basicity:
MgO(I) > MgO(IV) > MgO(VI) > MgO(V) > MgO(II) > MgO(III).
For strong basicity:
MgO(III) ≥ MgO(VI) > MgO(II) > MgO(I) ≥ MgO(IV) ≫ MgO(V).

Catalysts calcined at 750°C:

For total basicity:
MgO(IV) ≃ MgO(I) > MgO(V) ≥ MgO(VI) > MgO(II) ≫ MgO(III).
For strong basicity:
MgO(I) ≃ MgO(II) > MgO(VI) > MgO(IV) ≥ MgO(III) > MgO(V).

Catalysts calcined at 900°C:

For total basicity:
MgO(I) > MgO(V) > MgO(VI) > MgO(IV) > MgO(II) > MgO(III).
For strong basicity:
MgO(I) > MgO(II) > MgO(III) > MgO(VI) ≃ MgO(V) ≃ MgO(IV).

The results (Fig. 5) shows that total basicity is decreased with increasing calcination temperature. This is due to the sintering and annihilation of surface defects of the catalysts at higher temperatures. Among the catalysts studied, the lowest number of total basic sites are observed for the MgO (III) catalyst at all its calcination temperatures (i.e., 600, 750, and 900°C).

It may be noted that the MgO catalysts [viz., MgO(II), MgO(V), and MgO(VI)] contained a significant amount of CO_2 (which is expected to be present in the form of undecomposed Mg carbonate or strongly chemisorbed CO_2 or both). The basicity distribution data given in Figs. 4 and 5 were obtained by subtracting the CO_2 content from the experimentally observed STD data and hence may be considered as the lower limit of the basicity of the catalysts. The upper limit of the basicity of the catalysts could be obtained by adding the CO_2 content to the

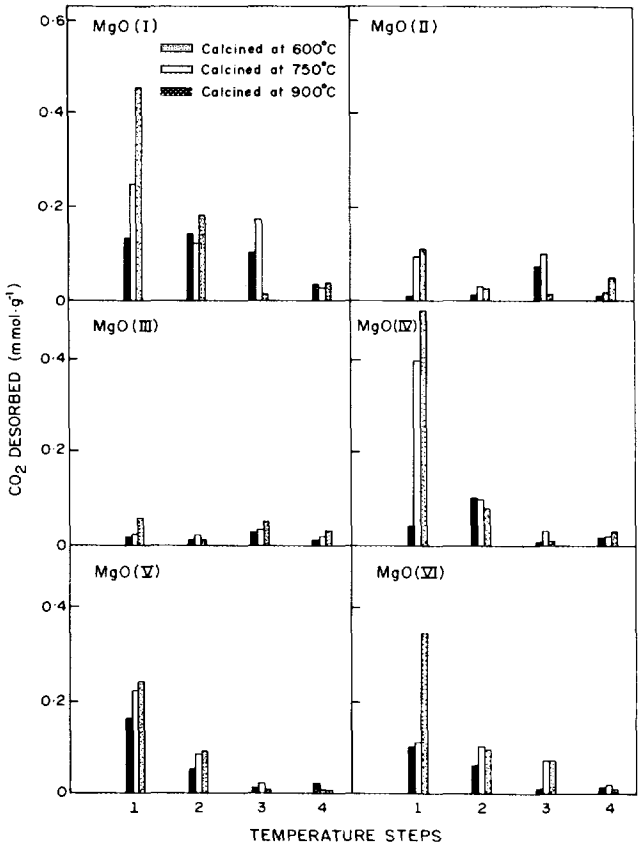

FIG. 4. Stepwise thermal desorption of CO_2 on MgO (I–VI) catalysts calcined at different temperatures Temperatures steps: (1) 50–250°C, (2) 250–500°C, (3) 500–700°C, and (4) 700–980°C (after subtracting CO_2 content data).

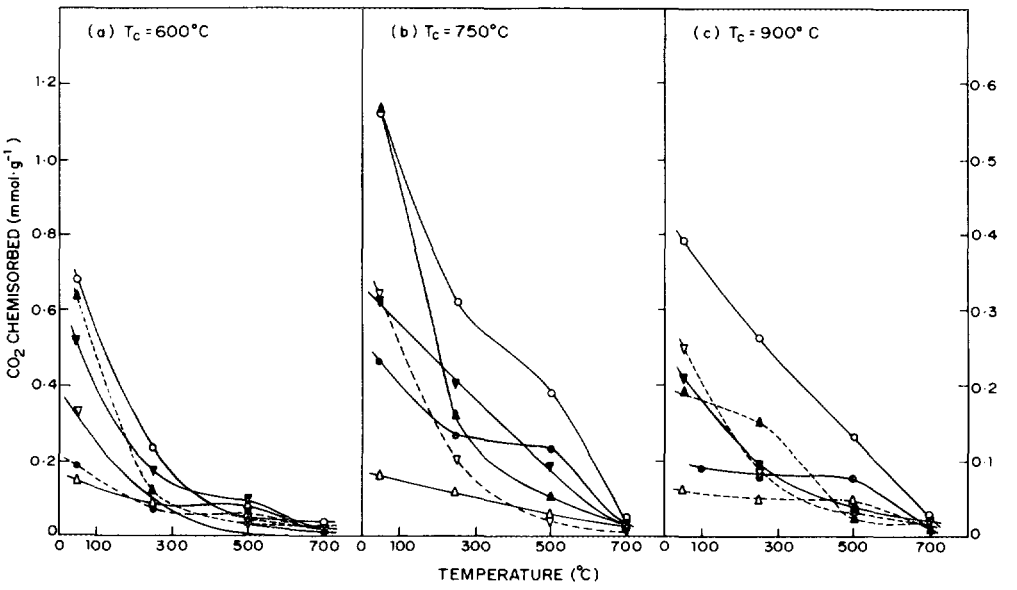

FIG. 5. Temperature dependence of chemisorption of CO_2 on MgO (I–VI) catalysts calcined at different temperatures (T_c = catalyst calcination temperature) MgO (I) [○], MgO (II) [●], MgO (III) [△], MgO (IV) [▲], MgO (V) [▽], and MgO (VI) [▼] (after subtracting CO_2 content data).

reported CO_2 chemisorption data. The exact values of CO_2 chemisorption on these catalysts could not be obtained because of the difficulty in determining the fraction of CO_2 content as chemisorbed CO_2 or bulk carbonate phase. At the lower (e.g., 600°C) and higher (e.g., 900°C) temperatures, the bulk carbonate, and chemisorbed CO_2, respectively, are expected to be predominant.

The acidity and basicity distributions studies reveal the presence of site energy distributions or groups of sites of different energies on the MgO catalysts studied. The acidity and basicity are attributed to the cations (Mg^{2+}) and anions (O^{2-}), respectively, exposed on the surface of the catalysts (30). Magnesium oxide has a highly defective surface structure showing steps, kinks, corners, etc., which provide Mg^{2+} and O^{2-} sites of low coordination (31). These differently coordinated Mg^{2+} and O^{2-} sites are responsible for the acidic and basic sites of different strengths, respectively. The lower the coordination number of the sites, the higher the strength of the site. The creation and annihilation of surface defects result in changes in the low-coordinated surface ions and consequently affect the acidity and basicity distributions on the MgO catalyst depending upon its conditions (viz., precursor used and its decomposition/calcination temperature).

Catalytic Activity/Selectivity in OCM

The OCM process over MgO (I–VI) catalysts (calcined at 900°C) was carried out at 700–850°C, CH_4/O_2 ratios of 3.0, 4.0, and 8.0, and GHSV of 25,500, 51,600, and 102,000 $cm^3 \cdot g^{-1} \cdot h^{-1}$ at atmospheric pressure.

The influence of reaction temperature on the methane conversion, C_2 selectivity, and C_2H_4/C_2H_6 product ratio in the OCM over the catalysts (for CH_4/O_2 = 4.0 and GHSV = 51,600 $cm^3 \cdot g^{-1} \cdot h^{-1}$) is shown in Fig. 6. The results reveal that with increasing temperature the methane conversion, C_2 selectivity, and C_2H_4/C_2H_6 ratio increase whereas the CO/CO_2 ratio decreases. An increase in the C_2 selectivity with temperature has been observed earlier in the OCM over La_2O_3 (32), Sm_2O_3 (33), $K–Sb_2O_4$ (34), and Li–ZnO–MgO (18) catalysts. The increase in the C_2 selectivity is expected to be mostly due to a decrease in the formation of carbon dioxide by gas-phase decomposition of methyl peroxy radicals ($CH_3OO\cdot$), of which the formation by gas-phase reaction of free oxygen with methyl radicals (formed at the catalysts surface) is not favored at higher temperatures (32). The increase in the ethylene/ethane ratio with temperature for all the catalysts suggests that the conversion of ethane [which is formed by coupling of methyl radicals (1)] to ethylene is favored at higher temperatures. The increase in ethylene/ethane ratio with the reaction temperature is consistent with that observed in earlier studies (32, 33, 35–38). The increase in C_2H_4/C_2H_6 ratio with increasing temperature is expected due to the decomposition of ethyl radicals and thermal cracking of ethane to ethylene at the higher temperatures. It may be also due to the increase in the rate of the oxidative dehydrogenation of ethane on the catalyst surface and also in the gas phase. For all the catalysts, the CO/CO_2 ratio decreases with increasing temperature. This indicates that the formation of CO_2 over that of CO is favored at the higher temperatures.

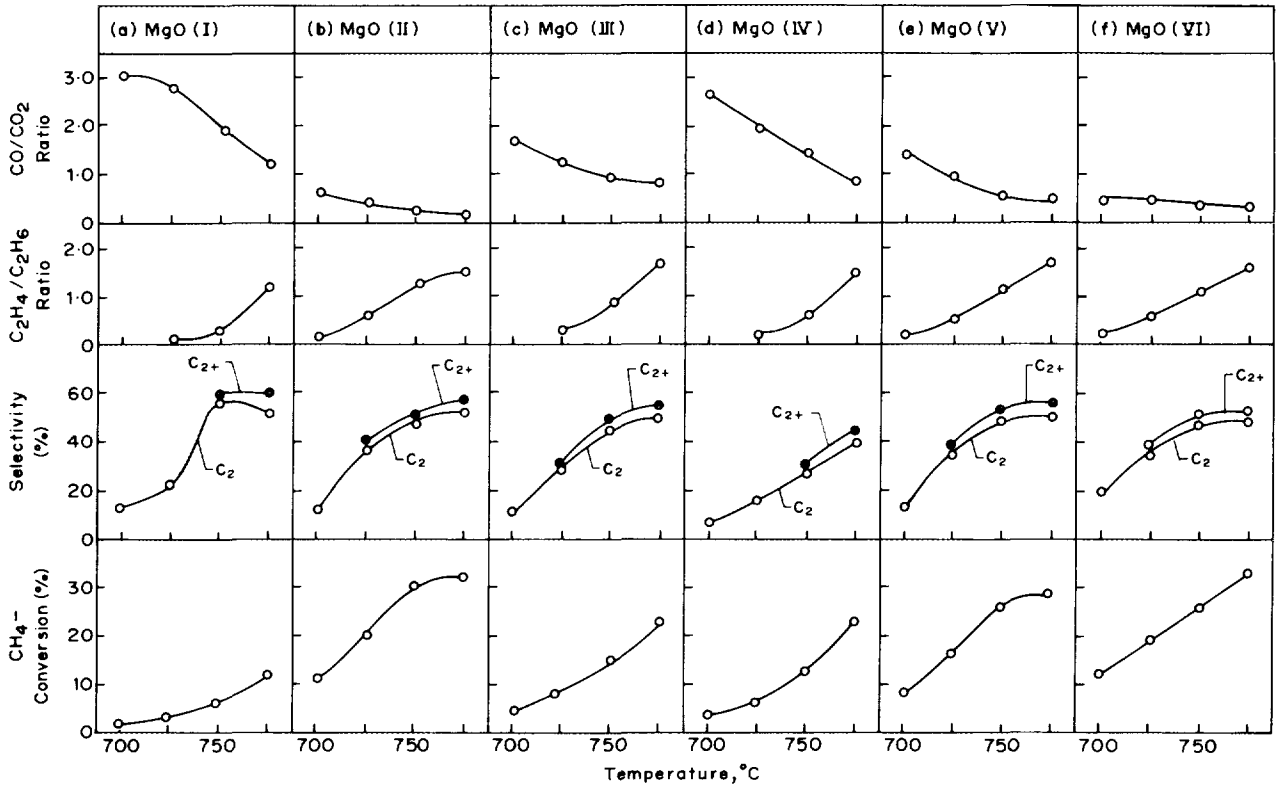

FIG. 6. Influence of temperature on CH_4 conversion, C_2 and C_{2+} selectivities, C_2H_4/C_2H_6 ratio, and CO/CO_2 ratio in OCM over MgO (I–VI) catalysts calcined at 900°C (CH_4/O_2 ratio = 4 and GHSV = 51,600 $cm^3 \cdot g^{-1} \cdot h^{-1}$).

The results in Fig. 7 show that when the CH_4/O_2 ratio in the feed increases the methane conversion and C_2H_4/C_2H_6 ratio decrease, and C_2 selectivity and CO/CO_2 ratio increase. The increase in the C_2 selectivity with decreasing O_2 concentration in the feed (or increasing CH_4/O_2 ratio) has also been observed earlier in the OCM over rare earth oxide catalysts (36) and La-promoted MgO (38). The increase in ethylene/ethane ratio with decreasing CH_4/O_2 ratio, which is also observed for the rare earth oxide catalysts (36), is most probably because of the availability of O_2 at higher concentration for the following gas-phase reactions involved in the formation of ethyl radicals and ethylene from ethane (40, 41):

$$C_2H_6 + O_2 \rightarrow C_2H_5\cdot + HO_2\cdot \quad [1]$$

$$C_2H_5\cdot + O_2 \rightarrow C_2H_4 + HO_2\cdot \quad [2]$$

$$C_2H_6 + HO_2\cdot \rightarrow C_2H_5\cdot + H_2O_2 \quad [3]$$

The increase in CO/CO_2 ratio with increasing CH_4O_2 ratio in the feed is, however, expected because of the fact that, at the lower concentration of O_2, the formation of CO over that of CO_2 (i.e., partial or incomplete combustion) is favored.

The effect of space velocity on the methane conversion, C_2 and C_{2+} selectivity, and C_2H_4/C_2H_6 and CO/CO_2 product ratios in the OCM over the MgO catalysts (at 800°C and CH_4/O_2 = 4.0) is shown in Fig. 8. The results reveal the following.

—Methane conversion on MgO (I), MgO (III), and MgO (IV) decreases with increasing GHSV, whereas for MgO (II) the methane conversion passes through a maximum at a GHSV of about 51,600 $cm^3 \cdot g^{-1} \cdot h^{-1}$ and, for MgO (V) and (VI) catalysts the influence of GHSV on the conversion is very small.

—For all the catalysts except MgO (III) there is an increase in the C_2 selectivity with increasing the GHSV. However, for MgO (III) there is no significant influence of GHSV on the selectivity.

—The ethylene/ethane ratio decreases with increasing GHSV, the decrease being very pronounced for MgO (I), (III), and (IV) catalysts. The decrease in ethylene/ethane ratio with increasing GHSV suggests that ethylene is formed in a consecutive reaction:

$$CH_4 \rightarrow C_2H_6 \rightarrow C_2H_4.$$

—The CO/CO_2 ratio for all the catalysts increases with increasing GHSV. This indicates that the formation of CO

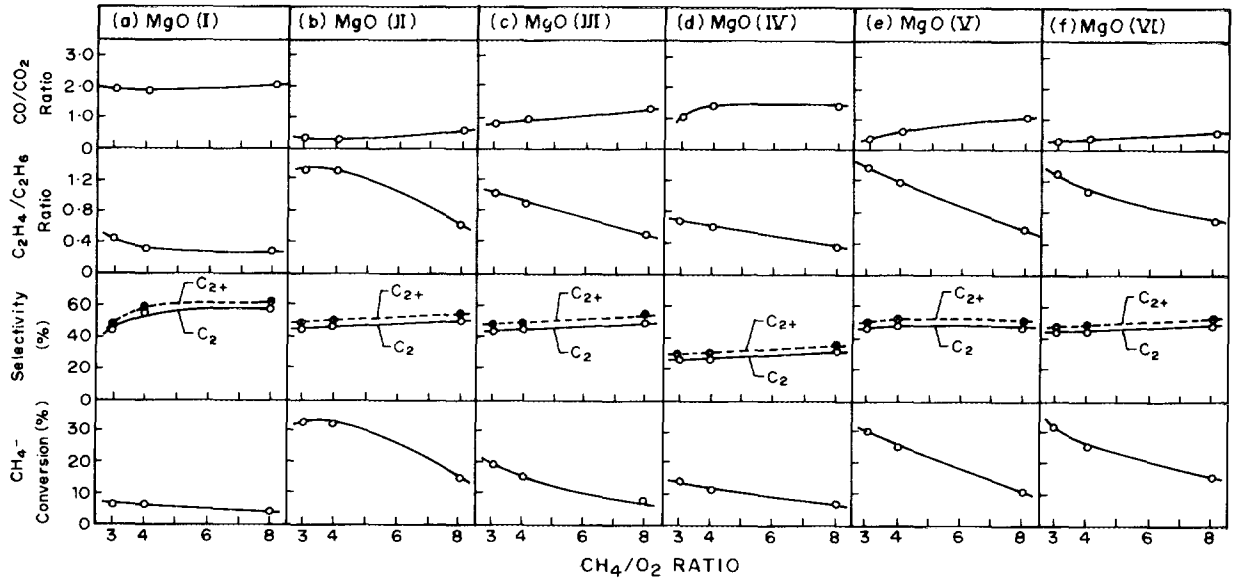

FIG. 7. Influence of CH_4/O_2 ratio on catalytic activity, selectivity and product ratios in OCM over MgO (I–VI) catalysts calcined at 900°C (GHSV = 51,600 $cm^3 \cdot g^{-1} \cdot h^{-1}$ and temperature = 800°C).

is favored at lower contact times and the CO_2 is formed, at least partly, from CO oxidation.

Comparison of MgO (I–VI) Catalysts for Their Surface and Catalytic Properties

The MgO (I–VI) catalysts (calcined at 900°C) are compared for their catalytic activity/selectivity in the OCM (at CH_4/O_2 = 4.0 and temperature = 800°C) in Table 3.

The catalysts could be arranged for their CO_2 content, total basicity (measured in terms of CO_2 chemisorbed at 50°C), strong basicity (measured in term of CO_2 chemisorbed at 500°C), surface acidity (measured in terms of NH_3 chemisorbed at 100°C), methane conversion, C_2-selectivity and C_2 yield in the following manner.

CO_2 content:

$$\text{MgO(II)} \gg \text{MgO(VI)} > \text{MgO(V)} \ggg \text{MgO(IV)} \simeq \text{MgO(III)} \simeq \text{MgO(I)}.$$

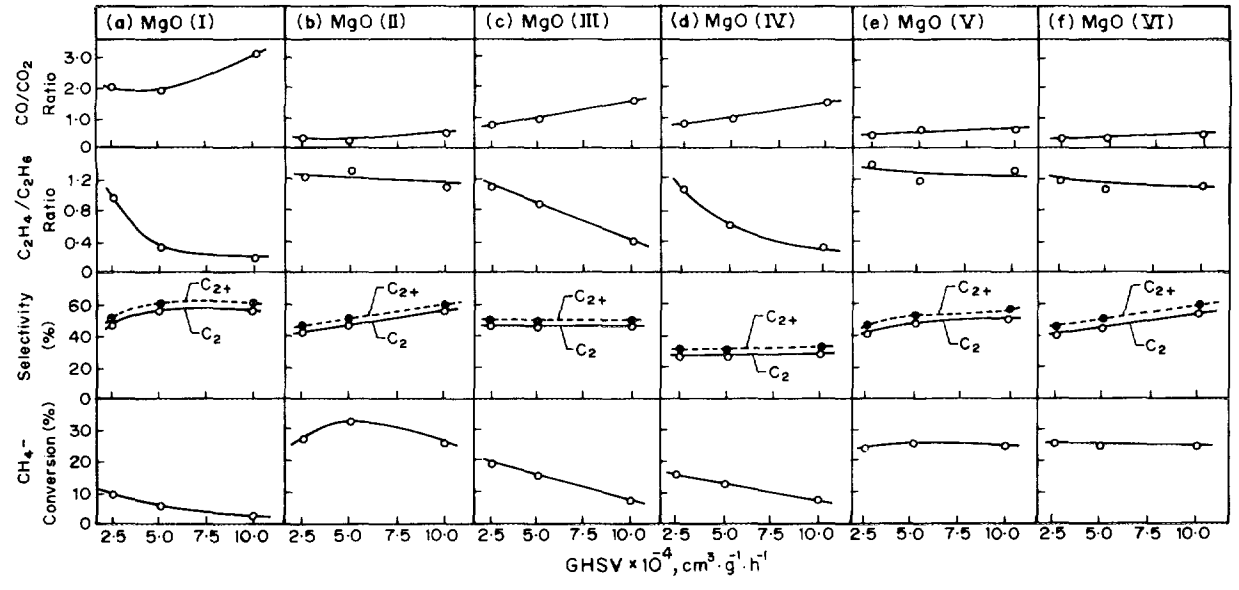

FIG. 8. Influence of GHSV on catalytic activity, selectivity and product ratios in OCM over MgO (I–VI) catalysts calcined at 900°C (CH_4/O_2 = 4.0 and temperature = 800°C).

TABLE 3

Comparision of MgO (I–VI) Catalysts (Calcined at 900°C) for their Catalytic Activity/Selectivity in the Oxidative Coupling of Methane

Catalyst	CO_2 content (mmol · g^{-1})	CH_4 conversion (%)	Selectivity (%)		C_2 yield (%)	C_2H_4/C_2H_6 ratio	CO/CO_2 ratio
			C_2	C_{2+}			
MgO (I)	0.0	2.6	47.3	47.8	1.2	0.19	3.12
MgO (II)	0.05	25.2	53.8	57.5	14.5	1.14	0.38
MgO (III)	0.0	6.8	45.0	46.6	3.2	0.41	1.50
MgO (IV)	0.0	7.0	29.6	30.3	2.1	0.31	1.78
MgO (V)	0.004	24.9	52.7	56.5	14.1	1.34	0.53
MgO (VI)	0.006	25.3	55.2	59.0	14.9	1.13	0.31

Note. Reaction conditions: temperature = 800°C, CH_4/O_2 ratio = 4.0, and GHSV = 102,000 $cm^3 \cdot g^{-1} \cdot h^{-1}$).

Total basicity:

(i) Lower limit (excluding the CO_2 content):

$$\text{MgO(I)} > \text{MgO(V)} > \text{MgO(VI)} > \text{MgO(IV)} > \text{MgO(II)} > \text{MgO(III)}.$$

(ii) Upper limit (including the CO_2 content)

$$\text{MgO(I)} > \text{MgO(V)} > \text{MgO(VI)} > \text{MgO(II)} > \text{MgO(IV)} > \text{MgO(III)}.$$

Strong basicity:

(i) Lower limit (excluding the CO_2 content)

$$\text{MgO(I)} > \text{MgO(II)} > \text{MgO(III)} > \text{MgO(VI)} > \text{MgO(V)} \simeq \text{MgO(IV)}.$$

(ii) Upper limit (including the CO_2 content)

$$\text{MgO(II)} > \text{MgO(I)} > \text{MgO(VI)} > \text{MgO(III)} > \text{MgO(V)} > \text{MgO(IV)}.$$

Total acidity:

$$\text{MgO(I)} \geq \text{MgO(V)} > \text{MgO(III)} \simeq \text{MgO(VI)} > \text{MgO(IV)} > \text{MgO(II)}.$$

Although MgO (I) has the highest acidity, it contains mostly weak acid sites. Whereas, the other MgO catalysts contain mainly intermediate strength acid sites and also to a small extent both strong and weak acid sites.

Methane conversion activity:

$$\text{MgO(VI)} \geq \text{MgO(II)} \geq \text{MgO(V)} \gg \text{MgO(IV)} \geq \text{MgO(III)} > \text{MgO(I)}.$$

C_2 selectivity:

$$\text{MgO(VI)} > \text{MgO(II)} \geq \text{MgO(V)} > \text{MgO(I)} > \text{MgO(III)} > \text{MgO(IV)}.$$

C_2 yield (methane conversion × C_2-selectivity/100):

$$\text{MgO(VI)} > \text{MgO(II)} > \text{MgO(V)} \gg \text{MgO(III)} > \text{MgO(IV)} > \text{MgO(I)}.$$

The above comparison reveals that the surface and catalytic properties of MgO are strongly dependent upon the precursor from which the MgO catalyst is prepared. The MgO catalysts obtained from magnesium acetate and magnesium carbonate showed much higher activity in the OCM than that shown by the catalysts obtained from hydrated MgO, magnesium hydroxide, and magnesium nitrate.

The above comparison of the MgO catalysts for surface and catalytic properties reveals that there is no direct correlation between the catalytic activity/selectivity and the acidity/basicity of the catalysts. However, the trends for CO_2 content and catalytic activity, C_2 selectivity, and C_2 yield are more or less similar. This indicates that the presence of CO_2 in the catalyst in the form of strongly adsorbed and/or adsorbed (i.e., occluded in the catalyst matrix) CO_2 has a beneficial effect on the catalytic activity/selectivity in the OCM process. In earlier studies on Li-promoted MgO (9), the high stability for catalytic activity and selectivity in the OCM process shown by the Li–MgO catalyst, prepared using Li and Mg acetates as catalyst precursors, was attributed to high CO_2 content, which stabilizes the catalyst against sintering and loss of Li during the process. An increase in the stability of Li–MgO due to addition of CO_2 at low concentration in the reaction mixture was also observed (4).

The MgO (II) (obtained from magnesium acetate) and

TABLE 4

Comparison of Catalytic Activity/Selectivity and Space–Time Yield (or C_2 STY) of MgO (II, V, and VI) Catalysts with Earlier MgO Catalyst Containing Different Promoters for OCM (at 750–800°C)

Catalyst	CH_4 conversion (%)	C_2 selectivity (%)	C_2 yield (%)	C_2 STY[a] (mmol · g^{-1} · h^{-1})	Ref.
Li (7 wt%)–MgO	29.1	58.1	16.9	0.3	(1)
Li–MgO (Li/Mg = 0.1)	20.0	70.4	14.0	55.2	(9)
Na (3 mol%)–MgO	31.0	47.7	14.8	65.4	(39)
K (3 mol%)–MgO	30.8	42.7	13.2	58.3	(39)
Rb (3 mol%)–MgO	30.2	37.7	11.4	50.4	(39)
Li^+–MgO–Cl^-	37.0	52.9	20.0	1.5	(8)
$CaCl_2$ (5 wt%)–MgO	26.6	59.4	15.8	14.5	(17)
Sm_2O_3(25 wt%)–MgO	16.5	57.0	9.4	20.8	(14)
La–MgO (La/Mg = 0.1)	29.2	60.3	17.6	161.4	(17)
Pb (0.4%)–MgO	13.1	51.0	6.7	92.3	(40)
PbO (20 wt%)–MgO	10.0	65.0	6.5	28.0	(15)
PbO (5 wt%)–MgO	19.2	60.4	11.6	106.4	(17)
MgO (II)	25.2	53.8	13.6	266.3	Present study
MgO (V)	24.9	52.7	13.1	256.5	Present study
MgO (VI)	25.3	55.2	14.0	274.1	Present study

[a] Calculated from the data as

$$\frac{\text{GHSV (cm}^3 \cdot \text{g}^{-1} \cdot \text{h}^{-1}) \times \text{mole fraction of methane in feed} \times C_2 \text{ yield(\%)}}{2 \times 22.4 \times 100}.$$

MgO (V) and (VI) (obtained from magnesium carbonate) are compared with earlier reported MgO catalysts containing different promoters (viz., Li, Na, K, Rb, Cl, $CaCl_2$, Pb, La, and Sm) for their methane conversion activity, C_2 selectivity, C_2 yield, and C_2 productivity (or C_2 space–time yield) in OCM (at 750–800°C) in Table 4. The comparison reveals that the MgO (II), (V), and (VI) catalysts (without promoter) not only show a comparable (or even higher in some cases) activity, C_2 selectivity, and C_2 yield in OCM, but also gave much higher C_2 space–time yield. The extraordinary performance of MgO (II), (V) and (VI) catalysts is attributed mostly to CO_2 content due to a use of a particular precursor (i.e., magnesium acetate and magnesium carbonate) in their preparation. It is also interesting to note that when the Li-promoted MgO (9, 28, 41), La-promoted MgO (41), and Sm-promoted MgO (28) catalysts were prepared by using magnesium acetate and/or magnesium carbonate as precursors for MgO, the resulting promoted MgO catalysts showed much better performance in the OCM process and also their performance was found to be better than that of the unpromoted ones [i.e., MgO (II), (V) and (VI)] (9, 28, 41). This clearly reveals the importance of the precursor of MgO used in the preparation of promoted MgO catalysts for the OCM process.

CONCLUSIONS

Surface properties (viz., acidity/acid strength distribution, basicity/base strength distribution, surface area, surface species, etc.) and catalytic activity/selectivity (in the OCM process) of MgO catalysts obtained by thermal decomposition of hydrated MgO, magnesium acetate, magnesium carbonate, magnesium hydroxide, and magnesium nitrate are strongly influenced by the precursor used in the catalyst preparation. The catalytic activity and selectivity of MgO obtained from magnesium acetate and magnesium carbonate are comparable and much higher than those observed for the MgO obtained from hydrated MgO, magnesium hydroxide, and magnesium nitrate. The MgO (without any promoter) prepared from magnesium acetate and magnesium carbonate shows a comparable or even a better performance (in OCM) than some of the earlier reported catalysts containing MgO with different promoters. The high activity/selectivity of MgO prepared from magnesium acetate and magnesium carbonate is attributed mostly the presence of CO_2 in the catalyst in the form of strongly adsorbed and/or adsorbed (i.e., occluded) CO_2.

REFERENCES

1. Ito, T., and Lunsford, J. H., *Nature* **314,** 721 (1985); Ito T., Wang J. X., Lin, C. H., and Lunsford, J. H., *J. Am. Chem. Soc.* **107,** 5062 (1985).
2. Kimble J. B., and Kolts, J. H., *CHEMTECH*, 501 (1987).
3. Moriyama, T., Takasaki, N., Iwamatsu, E., and Aika, K., *Chem. Lett.*, 1165 (1986).
4. Korf, S. J., Roos, J. A., DeBruijn, N. A., van Ommen, J. G., and

Ross, J. R. H., *J. Chem. Soc. Chem. Commun.*, 1433 (1987); *Catal. Today* **2,** 535 (1988).
5. Campbell, K. D., and Lunsford, J. H., *J. Phys. Chem.* **92,** 5792 (1988).
6. Choudhary, V. R., Akolekar, D. B., and Rajput, A. M., *in* "Recent Trends in Chemical Engineering" (B. D. Kulkarni, R. A. Mashelkar, and M. M. Sharma, Eds.) Vol. 1, p. 90. Wiley Eastern, New Delhi, 1987.
7. Korf, S. J., Roos, J. A., Veltman, L. J., van Ommen, J. G., and Ross, J. R. H., *Appl. Catal.* **56,** 119 (1989).
8. Hinson, P. G., Clearfield, A. C., and Lunsford, J. H., *J. Chem. Soc. Chem. Commun.*, 1430 (1991).
9. Choudhary, V. R., Chaudhari, S. T., and Pandit, M. Y., *J. Chem. Soc. Chem. Commun.*, 501 (1991).
10. Iwamatsu, E., Moriyama, T., Takasaki, N., and Aika, K., *J. Catal.* **113,** 25 (1988).
11. Choudhary, V. R., Chaudhari, S. T., Rajput, A. M., and Rane, V. H., *J. Chem. Soc. Chem. Commun.*, 555 (1989); *Res. Ind.* **34,** 258 (1989).
12. Seleznev, V. A., Kadushin, A. A., Tulenin, Yu. T., Choudhary, V. R., and Rajput, A. M., *in* "Recent Developments in Catalysis, 4th Indo-Soviet Seminar on Catalysis, Madras, Dec. 18–21, 1990," (B. Viswanathan and C. N. Pillai, Eds.), p. 441.
13. Shestov, A. A., Muzykantov, V. S., Tulenin, Yu, T., and Kadushin, A. A., *Catal. Today* **13,** 579 (1992).
14. Hamid, H. B. A., and Moyes, R. B., *Catal. Today* **10,** 267 (1991).
15. Asami, K., Hashimoto, S., Shikada, T., Fujimoto, K., and Tominaga, H., *Chem. Lett.*, 1223 (1986).
16. Bartek, J. B., Hypp, J. M., Brazdil, J. F., and Grasselli, R. K., *Catal. Today* **3,** 117 (1988).
17. Choudhary, V. R., Rane, V. H., and Chaudhari, S. T., *Catal. Lett.* **6,** 95 (1990).
18. Choudhary, V. R., Rajput, A. M., Akolekar, D. B., and Seleznev, V. A., *Appl. Catal.* **62,** 171 (1990).
19. Jones, C. A., Leonard, J. J., and Sofranko, J., *J. Energy Fuel.* **1,** 12 (1987).
20. Fujimoto, K., Hashimoto, S., Asami, K., and Tominaga, H., *Chem. Lett.*, 2157 (1987).
21. Fujimoto, K., Hashimoto, S., Asami, K., Omato, K., and Tominaga, H., *Appl. Catal.* **50,** 223 (1989).
22. Shastri, A. G., Chae, H. B., Bretz, M., and Schwank, J., *J. Phys. Chem.* **89,** 3761 (1983).
23. Phillips, V. A., Opperhayser, H., and Kolbe, J. L., *J. Am. Ceram. Soc.* **61,** 75 (1978).
24. Choudhary, V. R., and Pandit, M. Y., *Appl. Catal.* **71,** 265 (1991).
25. Choudhary, V. R., Pataskar, S. G., Choudhari, P. N., and Zope, G. B., unpublished work.
26. Choudhary, V. R., and Rane, V. H., *J. Catal.* **130,** 411 (1991).
27. Choudhary, V. R., and Rane, V. H., *Catal. Lett.* **4,** 101 (1990).
28. Rane, V. H., Ph.D. Thesis, University of Poona, 1992.
29. Lunsford, J. H., *Catal. Rev.* **8,** 135 (1973).
30. Tanabe, K., *in* "Catalysis Science and Technology (J. R. Anderson and M. Boudart, Eds.), Vol. 2, p. 231. Springer-Verlag, Berlin, 1981.
31. Che, M. J., and Tench, A. J., *Adv. Catal.* **31,** 77 (1982).
32. Lin, C., Campbell, K. D., Wang, J. X., and Lunsford, J. H., *J. Phys. Chem.* **90,** 534 (1986).
33. Otsuka, K., Jinno, K., and Morikawa, A., *J. Catal.* **100,** 353 (1986).
34. Lo, M. Y., Agarwal, S. K., and Morcelin, G., *J. Catal.* **112,** 168 (1988).
35. Chevalier, C., dala Piscina, P. R., Ceraso, M., and Choplin, A., *Catal. Today* **4,** 433 (1989).
36. Choudhary, V. R., Chaudhari, S. T., Rajput, A. M., and Rane, V. H., *J. Chem. Soc. Chem. Commun.*, 1526 (1989).
37. Morales, E., and Lunsford, J. H., *J. Catal.* **118,** 255 (1989).
38. Geisbrecht, R. A., and Daubart, T. E., *Ind. Eng. Chem. Process Des. Dev.* **14,** 159 (1975).
39. Matsuura, I., Utsumi, Y., and Doi, T., *Appl. Catal.* **47,** 299 (1989).
40. Agarwal, S. K., Migone, R. A., and Marcelin, G., *J. Catal.* **12,** 110 (1990).
41. Chaudhari, S. T., Ph.D. Thesis, University of Bombay, 1993.